JOURNAL OF PROPULSION AND POWER
Vol. 25, No. 2, March–April 2009

Probabilistic Aspects of Scramjet Design

Gerrit Schütte* and Stephan Staudacher†
Institute of Aircraft Propulsion Systems, 70569 Stuttgart, Germany

DOI: 10.2514/1.38195

Scramjet design is characterized by a multitude of design variables influencing a highly nonlinear and complex system. Methods such as mean line calculations, high fidelity computational fluid dynamics, and empirical studies are generally used to derive aircraft engine performance. Because of the high complexity and the incomplete knowledge of hypersonic flow regimes, the question of robust design arises in the given context and leads to the need of probabilistic methodology. In this paper a probabilistic approach to scramjet engine design assessing both inflow and model uncertainty is presented. The two different types of uncertainty are quantified with respect to their different nature by use of a two-step bootstrap methodology. A descriptive sampling Monte Carlo method is employed to propagate the quantified uncertainties through the engine model to exemplify the high sensitivity of net thrust vector to present uncertainties and to analyze the correlation between the parameters variations.

Nomenclature

A	=	area, m^2
$\bar{E}_i$	=	error vector of the ith component, $i \in [0; \quad 31; \quad 4,7 \quad ; 9]$ (see Fig. 1)
$F_{\text{net},x}$, $F_{\text{net},y}$	=	net thrust in x and y directions, N
$\bar{G}_i$	=	vector of geometrical parameters of the ith component, $i \in [0; \quad 31; \quad 4,7 \quad ; 9]$ (see Fig. 1)
h	=	duct height, m
L	=	segment length, m
Ma	=	Mach number
$\dot{m}$	=	mass flow, $\text{kg} \cdot \text{s}^{-1}$
$\mathbf{n}$	=	surface normal vector
p	=	static pressure, Pa
$p(x)$, $p(x \mid y)$	=	probability of x; probability of x assuming y
Re_x	=	Reynolds number
$\tilde{S}_{\text{fuel}}$	=	vector of fuel parameters (see Fig. 1)
T	=	static temperature, K
v	=	velocity, $\text{m} \cdot \text{s}^{-1}$
$\tilde{X}_i$	=	vector of deterministic flow parameters of the ith component, $i \in [0; \quad 31; \quad 4,7 \quad ; 9]$ (see Fig. 1)
$\bar{X}_i$	=	vector of probabilistic flow parameters of the ith component, $i \in [0; \quad 31; \quad 4,7 \quad ; 9]$ (see Fig. 1)
α	=	ramp angle, deg
δ^*	=	boundary-layer displacement thickness, m
μ	=	mean value
$\xi(x)$	=	spline describing the geometry of the nozzle expansion ramp
ρ	=	flow density, $\text{kg} \cdot \text{m}^{-3}$

I. Introduction

THE development of future single-stage-to-orbit or two-stage-to-orbit space transportation systems is accompanied by the design of hypersonic air breathing propulsion systems. High flight Mach numbers above Mach 7 demand a supersonic combustion ramjet concept to allow for a positive net thrust, but with increasing Mach numbers the complexity and sensitivity to small deviations from the design point of engine concepts also increase. In 2005 the German National Research Council (DFG) launched the research training group Graduiertenkolleg (GRK) 1095/1 program, which addresses the design of a scramjet propulsion system [1]. The scientific goal is to investigate the aerothermodynamic behavior of the system, whereupon the achievement of a positive net thrust is a key feature for the further appliance in space transportation.

Performance calculation as a prime issue of the presented work is usually done by performing mean line calculations based on deterministic computational fluid dynamics (CFD) or empirical studies. In the hypersonic flow regime several physical phenomena, for example, shock-boundary-layer interaction or boundary-layer transition, are still to be established in detail. As a result even high fidelity CFD codes deal with a certain model imperfection. The validation of CFD models is complicated as well, because existing wind tunnels are not able to provide free flight conditions at high Mach numbers regarding Reynolds, Mach, and Damköhler similarity at the same time. Beyond that, design calculations have to be performed with small effort regarding computing time and grid generation, and so further assumptions have to be implemented. From these simplifications and the lack of knowledge several model specific, so-called epistemic uncertainties arise that restrict the accuracy of any prediction made by this model. [Epistemic uncertainties (Greek: *episteme* = knowledge) arise from model imperfection. The terminus implies that specific assumptions becoming necessary during the modeling process are known to bias the result computed by the simplified model.]

Another source of uncertainty to account for is the aleatory uncertainty arising from imprecise forecast of the environmental input. [Aleatory uncertainties (Latin: *aleas* = dice) arise from the natural variance of input variables. The accuracy of these variables is restricted by the error of measurements and machining inaccuracies.] The flight conditions as well as performance parameters, for example, the fuel temperature, can only be measured with limited accuracy [2]. Following the previous discussion, the current approach replaces the deterministic single value solution by a probability density function (PDF) to account for model reliability and design robustness. Both natural variance of environmental parameters and model uncertainty are taken into account for the current analysis of the scramjet propulsion system.

II. Modeling Approach

Any probabilistic analysis is based on a deterministic model that provides the aerothermodynamical data of the scramjet engine and its performance characteristics in assumption of precise knowledge of

Presented as Paper 1811 at the 10th AIAA Non-Deterministic Approaches Conference, Schaumburg, IL, 7–10 April 2008; received 22 April 2008; revision received 4 August 2008; accepted for publication 11 August 2008.

*Ph.D. Student, Pfaffenwaldring 6; schuette@ila.uni-stuttgart.de. Member AIAA.

†Professor, Director, Pfaffenwaldring 6; staudacher@ila.uni-stuttgart.de.

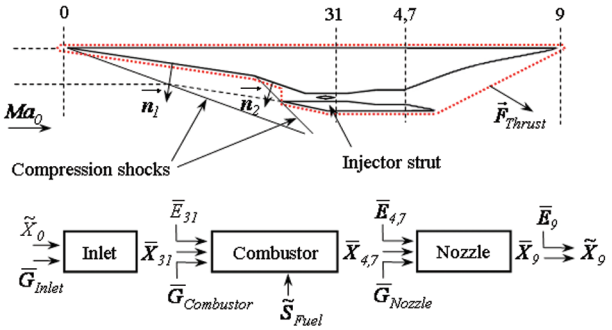

Fig. 1 Nomenclature and data flow of the LFM modular setup.

the physical processes. For probabilistic analysis a large number of simulations is required to achieve an acceptable reliability with respect to the sampled parameters uncertainties, and so the fidelity of the model must meet the computational time restrictions. In this context a modular structure is recommended. Accordingly the engine is subdivided into three parts (Fig. 1). The index 0 indicates the freestream conditions, and 31, 4,7 and 9 the outflow cross sections of the inlet, combustor, and nozzle, respectively.

For the specific modules different modeling approaches are chosen with respect to the modules function and integrated to the low fidelity model (LFM) of the scramjet. At the modules interface cross sections, the mass averaged flow properties are propagated to the following module. The vector $\bar{X}_i$ depicts the deterministic flow conditions and resulting forces whereas $\tilde{S}_i$ and $\bar{G}_i$ consist of performance parameters and geometrical data, respectively. Thus any module of the scramjet model can be treated as a black box with a PDF shaped input and a correspondingly PDF shaped output. Each modules output is propagated to the following module via Bayes's theorem with respect to the also PDF shaped model uncertainty [3]. This uncertainty is expressed by the error vectors $\bar{E}_i$ whose elements $\varepsilon_{i,j}(\mu,\sigma)$ represent the quantified uncertainty in the modules output flow parameters.

As a result each value used during computation assumes the shape of a probability density function whose mean value represents the calculations most probable result. The standard deviation is a measure for the expected scatter around the most probable result. This approach consisting of a deterministic model structure with probabilistic parameters permits a prediction of the most probable system performance combined with a statement to the forecasts reliability with respect to the combined epistemic and aleatory uncertainty.

A. Inlet/Nozzle

The main function of the inlet is the deceleration and compression of the captured air mass flow in order to achieve sufficiently high temperatures for autoignition in the combustor. The nozzle is characterized by an asymmetric shape with a large expansion ramp and a small flap. The asymmetric shape of the inlet and nozzle component leads to a vertical component in the net thrust vector. To depict the most important phenomena such as shock angles and wall pressure distributions within a reasonable computational time, the inlet and nozzle are described by a strictly inviscid 2-D Euler solution. Viscous effects are assessed by the geometrical addition of the compressible, turbulent boundary-layer displacement thickness

$$\delta^* = 0.046 \cdot (1 + 0.8 \cdot Ma^2)^{0.44} \cdot x \cdot Re_x^{-1/5}$$

to the geometric wall [4,5]. A discontinuous Galerkin finite element scheme is used to solve the inviscid compressible Euler equations in two spatial dimensions on unstructured meshes. The solving algorithm provides an automatic mesh refinement option depending on the evolved flowfield to keep the initial mesh as sparse as possible [6].

B. Combustor

The combustor module describes the chemical reactions during fuel mixing, ignition, and burning. As the combustor shows a symmetric shape, a 1-D flow computation is applied to reduce processing time. The flow computation is combined with a Research and Development (RAND) [7] algorithm solving a 12-species reaction scheme to model the thermochemical effects of ignition and combustion. Viscous effects are addressed the same way as done for the inlet/nozzle model but additionally the total temperature loss due to wall heat fluxes is considered. The local mixing of fuel and oxidizer is approximated by an exponential mixing rule

$$\eta_{\text{mix}} = 1 - e^{\frac{\ell_n(1-\eta_{\max})\cdot x}{L_{\text{mix}}}} \tag{2}$$

where η_{mix} depicts the local mixing efficiency, and $\eta_{\max}$ the ideal mixing efficiency after an ideal mixing length L_{mix} [8]. Recent studies indicate the existence of two different modes of combustion, where only strong combustion is taken into account in this context [9]. Although the ignition behavior of the strong combustion mode is mainly influenced by the high temperature in the wake of the horizontal injector strut, the combustion model follows a two-step procedure. In the first step the ignition delay is computed using nonequilibrium chemistry within the hot shear layer in the direct wake of the strut. The computation of the heat addition due to combustion of the injected fuel follows in a second step using the mass averaged gas properties at the combustor entrance cross section and the ignition delay provided by the first step.

III. Uncertainty Quantification and Propagation

As mentioned previously the hypersonic flow regime is affected by uncertainties of two different kinds arising from model imperfection or limited measurement capability. Although their variability is owed to different sources, aleatory and epistemic uncertainty must be treated in a different manner [10].

A. Quantification Procedure

Former approaches apply Bayes's theorem for uncertainty quantification by merging experimental data with an a priori hypothesis to get an a posteriori information about the model accuracy [11]. Following Laplace's principle of insufficient reason this hypothesis must meet the demands of the maximum entropy method. Therefore the a priori hypothesis holds for a very high uncertainty that is reflected in a high standard deviation of that initial estimation [12]. The successive Bayesian update scheme converges for a sufficient number of data against the real model uncertainty disregarding the initial hypothesis. Following the discussion in [13] the Berry–Esséen theorem leads to a weak rate of convergence of Bayesian update schemes. As the amount of reliable data is sparse, the results provided using this approach will be dominated by the initial hypothesis, which disqualifies Bayes's theorem for the use for uncertainty quantification in this special case. Other approaches using evidence theory or polynomial chaos show better performances regarding their global convergence, but have not yet reached a state of practicability [14,15]. In this paper a two-step methodology is introduced to quantify the *local* model uncertainty in the direct physical proximity of the investigated configuration without anticipating hypotheses.

In the first step the measurement uncertainty of the available experimental data is assessed and the numerical high fidelity model (HFM) is calibrated using the experimental data. This leads to a stochastic residual error of the high fidelity model which is given by the measurement uncertainty of the experimental data. It is assumed that this stochastic residual error dominates the epistemic uncertainty of the calibrated high fidelity model. Assuming that the measurement noise is owed to a large number of factors again with different PDF shaped noises, Lyapunov's central limit theorem yields a Gaussian shaped distribution of this residual error [16,17].

In the second step the LFM is compared to the calibrated high fidelity model at several points within a range which ensures physical similarity. As the difference between HFM and LFM is owed to

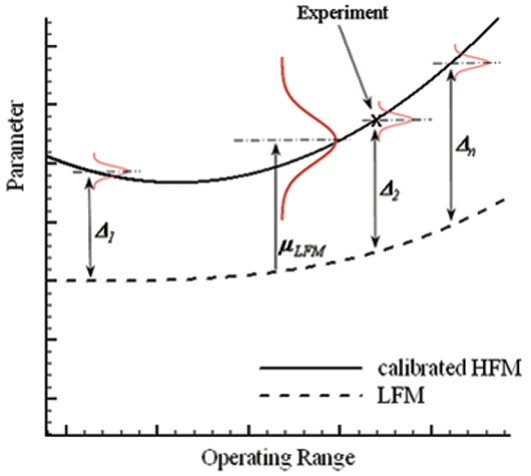

Fig. 2 Methodology of uncertainty quantification.

epistemic uncertainty this second step uncertainty is not subject to random variance. The stochastic nature of this uncertainty comes from small changes in the operating range affecting the parameter value due to effects that are not assessed by the LFM. These effects are covered by the stochastic interpretation of the particular parameter. The procedure is shown in Fig. 2.

Assuming that the calibrated HFM represents the real value in the direct physical neighborhood of the experiment, the probability density function of the LFM error is defined by

$$\mu_{\mathrm{LFM}} = \frac{\sum_{j=1}^{n}(x_{\mathrm{HFM}} - x_{\mathrm{LFM}})_j}{n} \tag{3}$$

and

$$\sigma_{\mathrm{LFM}} = \sqrt{1/n \cdot \sum_{j=1}^{n}[(x_{\mathrm{HFM}} - x_{\mathrm{LFM}})_j - \mu_{\mathrm{LFM}}]^2} \tag{4}$$

where x_{HFM} and x_{LFM} depict the respective flow parameter computed by the high fidelity model and the low fidelity model, respectively, for n available HFM data sets. This bootstrap estimation of the uncertainties distribution assumes further Gaussian shape. The Kullback–Leibler [18] distance between the assumed Gaussian distribution and the student distribution tends to zero for increasing n. The applied location parameters of the maximum likelihood estimation were obtained from Eqs. (3) and (4). For a small amount of data ($n < 10$) this standard deviation expresses the *lower bound* of the occurring scatter. The overall error distribution of the model uncertainty is defined by the sum of the two PDF's derived in the two steps of the procedure. They are combined by the use of the convolution integral

$$\varepsilon_{i,j} = p(c) = p_{\mathrm{HFM}}(a) + p_{\mathrm{LFM}}(b) = \int_{-\infty}^{+\infty} p_{\mathrm{HFM}}(a) \cdot p_{\mathrm{LFM}}(c - a)\,\mathrm{d}x \tag{5}$$

where p_i denotes the probability distribution of the considered flow parameter with the corresponding arguments a, b, and c representing the distributions respective location parameters [19].

B. Quantification Data

The experimental results as well as the HFM data applied in the presented work are produced by the members of the above mentioned research program GRK 1095/1 and their associates. They are discussed in detail in the cited literature.

For the inlet module the experimental data from wind-tunnel tests at the German Aerospace Center (DLR) Cologne serve for HFM calibration [20,21]. The employed high fidelity models are an advanced Reynolds-averaged Navier–Stokes solver (FLOWER),

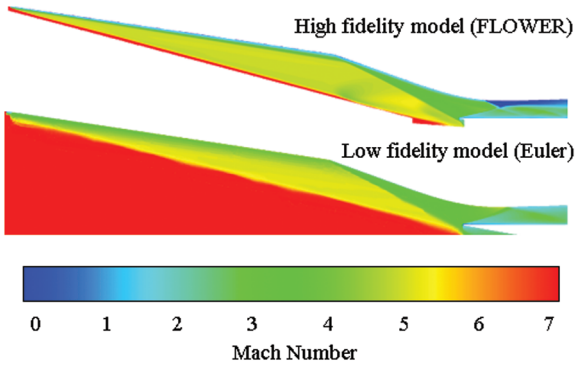

Fig. 3 Mach number distribution of the inlet flowfield.

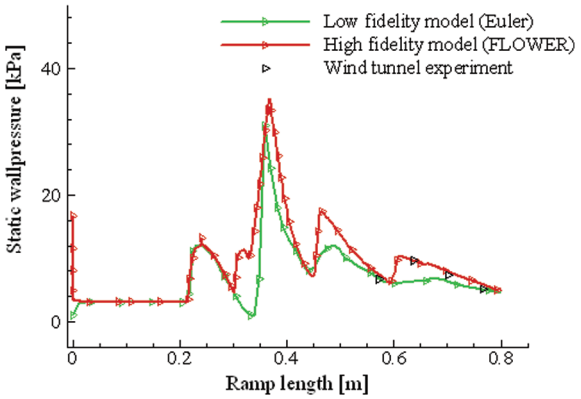

Fig. 4 Spatial pressure distribution on inlet compression ramp.

evaluated for three similar geometries and flow conditions using several different boundary-layer models [22]. The combustor modules uncertainty is quantified using the results from actual experiments and high fidelity numerical investigations applied for the recent studies of the turbulent reactive supersonic flows in the wake of lobed horizontal injector struts [23–25]. Correspondingly the uncertainty of the nozzle module is quantified by wind-tunnel data and the appropriate numerical studies [26].

In Fig. 3 the comparison of the high fidelity model solution and the low fidelity solution for the inlet module is depicted for an example geometry and flow condition.

Good agreement is obtained in the case of the compression shock position, but as expected for an Euler solution, boundary-layer effects are not considered in the LFM. This affects, in particular, the ramp side boundary-layer separation due to the interaction of the cowl shock with the boundary layer and must be regarded as one of the most important sources of epistemic uncertainty. The spatial pressure distribution on the inlets compression ramps for the two applied models in comparison with the wind-tunnel data is shown in Fig. 4. As implied by the Mach number distribution depicted in Fig. 3 the static ramp pressure computed by the HFM offers a quantitative difference to the LFM result in regions of boundary-layer separation (Fig. 4, $x = 0.35$ m). In the regions with attached boundary layers and especially in the outflow cross section, good agreement is obtained between the LFM result, the HFM result, and the wind-tunnel data.

However, the above procedure yields a mean error of $\mu = -0.3973$ for the low fidelity model with a corresponding overall standard deviation $\sigma = 0.2079$ for the Mach number and a mean error of $\mu = 0.0182$ with a corresponding overall standard deviation $\sigma = 0.1361$ for the static pressure. The other modules uncertainty PDFs are quantified in a similar way; their location parameters are summarized in Table 1. The model uncertainty which is shown in Table 1 is used to express the numerical results of a module in terms of a mean value and the model uncertainty

Table 1 Model uncertainty

Vector	ε	Location parameter μ	σ
E_{31}	$\dot{m}_{31}$, kg/s	0.0619	0.0361
	Ma_{31}, ——	−0.4767	0.2079
	T_{31}, K	50.8518	64.8791
$E_{4,7}$	$\rho_{4,7}$, kg/m^3	−0.00179	0.00059
	$Ma_{4,7}$, ——	0.0943	0.00115
	$T_{4,7}$, K	30.875	9.9066
E_9	$F_{\text{net},x}$, N	−63.5250	44.5081
	$F_{\text{net},y}$, N	−118.8392	97.6678

$$\tilde{X}_{31} = \bar{X}_{31} + \bar{E}_{31} = \begin{pmatrix} \dot{m} \\ Ma \\ T \end{pmatrix}_{31} + \begin{pmatrix} \varepsilon_{\dot{m}}(\mu,\sigma) \\ \varepsilon_{Ma}(\mu,\sigma) \\ \varepsilon_{T}(\mu,\sigma) \end{pmatrix}_{31} \tag{6}$$

for the inlet module,

$$\tilde{X}_{4,7} = \bar{X}_{4,7} + \bar{E}_{4,7} = \begin{pmatrix} \rho \\ Ma \\ T \end{pmatrix}_{4,7} + \begin{pmatrix} \varepsilon_{\rho}(\mu,\sigma) \\ \varepsilon_{Ma}(\mu,\sigma) \\ \varepsilon_{T}(\mu,\sigma) \end{pmatrix}_{4,7} \tag{7}$$

for the combustor module, and

$$\tilde{X}_{9} = \bar{X}_{9} + \bar{E}_{9} = \begin{pmatrix} F_{\text{net},x} \\ F_{\text{net},y} \end{pmatrix}_{9} + \begin{pmatrix} \varepsilon_{Fx}(\mu,\sigma) \\ \varepsilon_{Fy}(\mu,\sigma) \end{pmatrix}_{9} \tag{8}$$

for the nozzle module where both deterministic flow property vector $\bar{X}_i$ computed by the ith module and error vector $\bar{E}_i$ consisting of the specific $\varepsilon_{i,j}$ take the form of a PDF.

The treatment of the environmental data and the performance parameters is slightly different as their uncertainties do not include epistemic aspects. It follows the scheme

$$\tilde{X}_0 = \begin{pmatrix} \rho_0(\mu,\sigma) \\ Ma_0(\mu,\sigma) \\ AoA_0(\mu,\sigma) \\ T_0(\mu,\sigma) \end{pmatrix} \tag{9}$$

$$\tilde{S}_{\text{Fuel}} = \begin{pmatrix} \text{ER}(\mu,\sigma) \\ T_{\text{Fuel}}(\mu,\sigma) \\ v_{\text{Fuel}}(\mu,\sigma) \end{pmatrix} \tag{10}$$

where for those variables the mean value μ is defined by the deterministic value and the standard deviation σ corresponds to the error of measurement. Former investigations show that the low accuracy in environmental data acquisition leads to significantly high standard deviations that dominate the scramjet behavior and therefore restrict the significance of the correlations between the model uncertainty and the design robustness [2]. To avoid predominant flight condition uncertainty only the deterministic value is derived from the international standard atmosphere at 30 km altitude. According to custom procedures in free flight tests, the uncertainty affecting the parameters of the flight conditions is quantified by the use of registering balloon data. As the employed measuring devices are not exposed to hypersonic flow conditions and the corresponding high temperatures, a higher accuracy can be achieved by that approach. The data sheets of the applied pressure and temperature gauges and a conventional air data boom yield the values listed in Table 2 [27–29].

Concerning the performance parameters the accuracy of the liquid hydrogen mass flow measurement yields a standard deviation of 0.0033. The static fuel temperature is calculated based on temperature measurements during wind-tunnel experiments. A simplified estimation of the heat transfer from the hot strut to the fuel mass flow has been carried out. From the applied experiments a mean static fuel temperature of 409 K is obtained and the underlying experiment data variation leads to a standard deviation of 0.037. The uncertainty of injected fuel velocity is assessed by the geometrical variance of the Laval nozzle contour inside the strut during the experiments. All values are summarized in Table 3.

Table 2 Flight condition uncertainty; international standard atmosphere (ISA)

Vector	Element	Location parameter μ (ISA)	σ
$\tilde{X}_0$	ρ_0, kg/m^3	0.018012	5.3065×10^{-7}
	Ma_0, ——	8	0.0045
	AOA_0, ——	0	0.5
	T_0, K	226.65	0.0066

Table 3 Performance parameter uncertainty

Vector	Element	Location parameter μ	σ
$\tilde{S}_{\text{Fuel}}$	ER, ——	——	0.0033
	T_{Fuel}, K	409	0.0664
	v_{Fuel}, m/s	3081.56	0.0602

C. Uncertainty Propagation Method

The epistemic and aleatory uncertainties have to be propagated through the system analysis. Assuming an input vector of each module takes the form of a probability density function, each element of the output vector of each module also must be assumed to be a distributed variable. As the quantified model uncertainty is also given by a probability density function, the propagation via Bayes's theorem yields

$$p_{\text{input}}(\bar{X}_i) \propto p_{\text{output}}(\bar{X}_{i-1}) \circ p(\bar{E}_{i-1}) \tag{11}$$

where the a posteriori information $p_{\text{input}}(\bar{X}_i)$ represents the PDF of the ith modules input vector. It is given by the a priori information $p_{\text{output}}(\bar{X}_{i-1})$ of the previous modules output vector and the PDF of this modules error vector $p(\bar{E}_{i-1})$ [11].

To maintain the black box view of the defined modules, a Monte Carlo simulation methodology is applied to propagate the quantified uncertainties of model accuracy and flight condition correctly.

IV. Engine Configurations and Computational Setup

The scramjet engines basic configuration includes a 2-D external compression inlet with a horizontal cowl. For the combustor, a generic geometry with three segments of different lengths and different divergence angles is applied. The fuel is injected streamwise in the wake of a lobed horizontal injector strut with excellent mixing and flame holding capacities. An asymmetric single expansion ramp nozzle is applied for thrust generation. The nozzle expansion ramp is defined by a nonparametric spline derived from a method of characteristics for a horizontal exit flow angle [30]. The coordinates of the flaps trailing edge are defined by the combustor outflow cross section and the overall length of the engine and therefore are not independent variables.

In this study the combinations of two inlet designs, four combustor designs, and one nozzle design have been investigated. The first inlet design follows the initial assumptions of the GRK 1095/1 whereas the second one is derived involving optimizing criteria regarding ramp angles and contraction ratio to reduce the inlet drag [31] (Table 4).

The medial segment of the combustor shows a divergent shape to reduce the risk of thermal choking due to heat addition. Thermal choking is referred to as the occurrence of a normal shock in the combustor which is caused by increasing temperature and therefore decreasing Mach number. The segments lengths were varied as well

Table 4 Inlet configuration parameters

Module	Parameter	Description	Values	
			Initial	Modified
Inlet	α_1, deg	First ramp angle	7.5	6.25
	α_2, deg	Second ramp angle	11.5	7.75
	A_0/A_{31}, ——	Contraction ratio	6.0	5.0
	h_{31}, m	Interface height	0.038	0.038
	L_{iso}, m	Isolator length	0.1	0.1
	α_{iso}, deg	Isolator divergence angle	1	1

as the divergence angle of the medial segment whereas the total length of the combustor remains constant (Table 5).

The applied configuration of the nozzle module is outlined in Table 6.

To reduce computational effort and to ensure a complete reproducibility a descriptive sampling Monte Carlo method is applied [32]. From Bernoulli's law of large numbers it is known that for a sufficiently large number of realizations a simulation's result converges toward its real distribution.

The investigated case shows a good convergence for a number of 5000 individual simulation runs for each design configuration (Fig. 5). For a further increased number of runs no significant improvement is obtained.

As the individual runs of a Monte Carlo simulation are independent of each other the individual computational runs can be distributed to individual CPU's. For the presented investigations a cluster of 16 CPU's has been applied. In this way a number of 5000 runs could be performed within two days time.

V. Results and Discussion

In a first step the results of a deterministic computation of the mentioned configurations are compared. In Fig. 6 the absolute value of resulting net thrust in flight direction is plotted in dependency of the equivalence ratio (ER) for different combustor shapes combined with the initial inlet design defined by $\alpha_1 = 7.5$ deg, $\alpha_2 = 11.5$ deg, and a contraction ratio of 6.

For low equivalence ratios a proportional ascent is observable with the influence of the combustor shape being secondary. This ascent flattens slightly with increasing equivalence ratios for the combustors with a long first segment $L_1 = 0.3$ m and is truncated at an equivalence ratio of 0.52 due to thermal choking. By applying combustor shapes with a short first segment $L_1 = 0.1$ m higher equivalence ratios can be realized leading to a higher net thrust.

An immediate rise of the net thrust is observed at an equivalence ratio of 0.62 for the combustor design described by segment lengths of 0.1, 0.1, and 0.3 m and divergence angles of 0, 2, and 0 deg, respectively (Fig. 6). This phenomenon is owed to the fact that the fuel ignition is a function of static flow temperature, depending on the combustor shape, and of the equivalence ratio. As a result the ignition moves upstream for increasing equivalence ratios into the nondivergent part of the combustor, where the heat addition causes a stronger pressure rise that is reflected in a stronger ascent in the net thrust. This is confirmed by the fact that the maximum equivalence ratio for the combustor design with the higher divergence ($\delta_2 = 3$ deg) of 0.7 is higher than for the slender combustor ($\delta_2 = 2$ deg) that chokes at an equivalence ratio of 0.67.

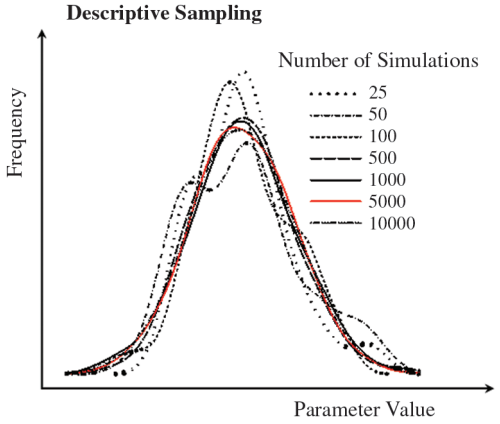

Fig. 5 Convergence of the descriptive sampling method.

For the computations outlined in Fig. 7 a modified inlet design is applied to reduce overall drag. This is achieved by lower ramp angles of $\alpha_1 = 6.25$ deg and $\alpha_2 = 7.75$ deg, respectively, and a lower contraction ratio of 5.0. To obtain comparable mass flow rates for a fixed combustor entrance height of 0.038 m the overall length of the inlet increases. As a result the increasing boundary-layer displacement thickness causes a higher spillage drag which leads to a reduction of overall efficiency. However, the deterministically obtained net thrust increases for any combustor shape considered in this study.

In addition the modified inlet design leads to an increased range of equivalence ratios without choking. Furthermore a higher net thrust gradient above the critical equivalence ratio is observed. This implies a higher sensitivity of the system at equivalence ratios from 0.59 to 0.73. The reason for the steeper gradient is the weaker compression of the modified inlet. Because of the more acute ramp angles the mass averaged temperature in the inlet outflow cross plane is lower. This causes, in combination with the higher Mach number, a stronger ignition delay, but the fuel mixing efficiency remains constant. As a result the reaction after ignition is more intense leading to the observed sensitivity to the equivalence ratio. The increased ignition delay has no significant effect on the overall combustion efficiency, because the mixing efficiency is the dominating factor for the long combustion chamber which was applied for this investigation.

A different pattern is obtained if the combination of epistemic and aleatory uncertainty is integrated (Fig. 8). As the main influence on net thrust is owed to the changes in inlet design, only one representative combustor design was investigated in combination with the different inlet geometries. This design is defined by a first segment length of 0.1 m and a divergence angle of the middle segment of 2 deg. It was found that for the initial inlet design at low equivalence ratios a Gaussian distribution is established. A maximum likelihood estimation of net thrust probability leads to a

Table 6 Nozzle configuration parameters

Module	Parameter	Description	Values
Nozzle	$\xi(x)$, m	Expansion ramp	Spline
	(x_F/y_F), m	Flap's trailing edge coordinates	——

Table 5 Combustor configuration parameters

Module	Parameter	Description	Values			
Combustor	L_1, m	First segment length	0.1	0.3	0.1	0.3
	L_2, m	Second segment length	0.1	0.1	0.1	0.1
	L_3, m	Third segment length	0.3	0.1	0.3	0.1
	δ_1, deg	First segment divergence angle	0.0	0.0	0.0	0.0
	δ_2, deg	Second segment divergence angle	2.0	2.0	3.0	3.0
	δ_3, deg	Third segment divergence angle	0.0	0.0	0.0	0.0

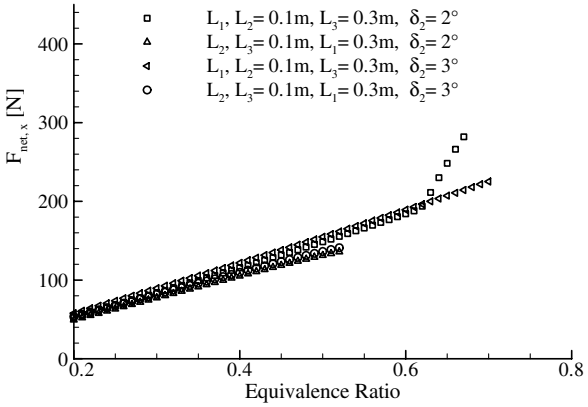

Fig. 6 Comparison of net thrust trend for different combustor shapes, initial inlet design.

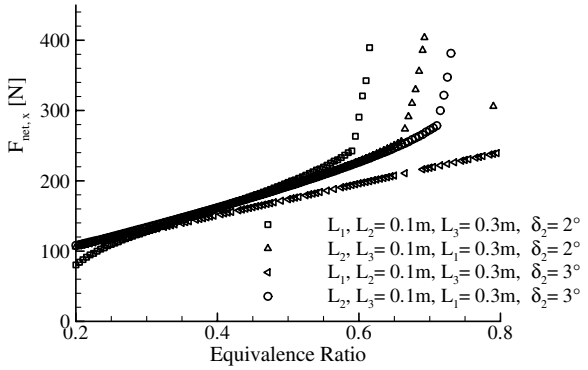

Fig. 7 Comparison of net thrust trend for different combustor shapes, modified inlet design.

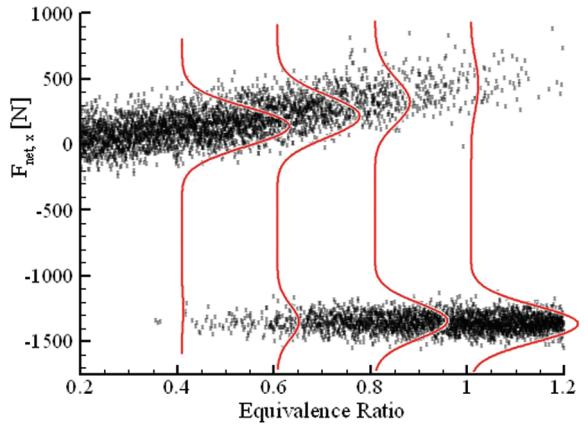

Fig. 8 Scatter view and corresponding PDFs for the initial inlet design.

mean value of 130.4 N and a standard deviation of 113.4 for $ER = 0.4$ (Table 7). For low equivalence ratios the obtained net thrust standard deviation is of the same order of magnitude as the observed mean value. This documents the risk of not achieving positive net thrust for this class of designs.

To increase the probability of a positive net thrust, higher equivalence ratios must be realized. At equivalence ratios of 0.6 or higher a bimodal distribution develops with the first peak describing the net thrust in the x direction and the second peak describing the vehicle drag for a choked combustor. An increased risk of thermal choking is observed for increasing equivalence ratios. In cases with choked combustor a mean net thrust of −1344.5 N is observed. The scatter is owed to the deviations in the applied flight conditions. For an equivalence ratio of 0.6 a risk of thermal choking of 17.3% is obtained with a mean net thrust of 214.6 N and a standard deviation

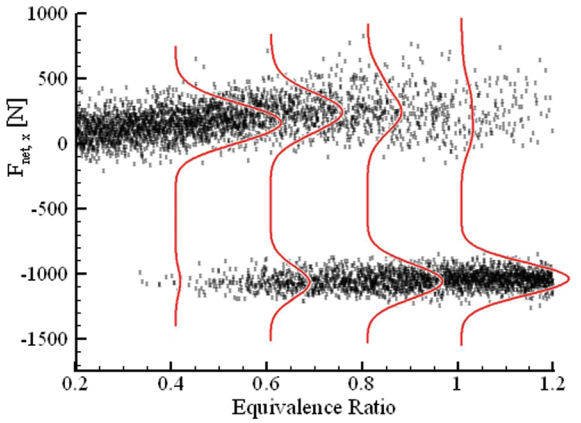

Fig. 9 Scatter view and corresponding PDFs for the modified inlet design.

of 112.7. At this equivalence ratio a comparison of the mean value with the deterministic prediction of 184.3 N shows that the mean of the probabilistic prediction is higher than the deterministic prediction. This is owed to the fact that the maximum net thrust is obtained immediately before thermal choking occurs. The involved uncertainties of the flight conditions and the inlets model uncertainty shift the obtained net thrust mean value to higher values until the constraint of thermal choking is reached. Hence, equivalence ratios higher than 0.8 can be realized but the probability of thermal choking increases massively. At an equivalence ratio of 1.0 a mean net thrust of 459.2 N is obtained with a standard deviation of 131.5. But the included risk of 91.3% for thermal choking puts that result into perspective.

Although the probabilistic trend of net thrust versus equivalence ratio follows the deterministic prediction for the initial inlet design, a different behavior is observed for the modified inlet design. For the modified inlet the development of a bimodal distribution can be observed also. The investigation of the modified inlet shows no monotonic increase in the mean value of net thrust (Fig. 9).

The mean value of net thrust increases for equivalence ratios up to about 0.8. For higher equivalence ratios a slight drop in the mean value of net thrust is predicted. The inlet drag is reduced from −1344 N to −1040 N for the modified inlet. The mean values of net thrust of the modified intake are higher than those of the initial inlet only at low equivalence ratios. An equivalence ratio of 0.6 results in a mean value of net thrust of 247.2 N for the modified inlet and 214.6 N for the initial inlet design. An increased equivalence ratio of 0.8 results in a mean net thrust of 303.9 N for the modified inlet and 346.8 N for the initial inlet design. Furthermore the obtained standard deviations increase for higher equivalence ratios and are significantly higher for the modified inlet geometry (Table 7).

The reason for that can be found in the higher sensitivity of the modified inlet to variations in the angle of attack (AoA). A covariance of 12.11 between the net thrust and the angle of attack is obtained here while the initial inlet design leads to a covariance of 9.57. The probabilistic investigation of the two configurations shows significant differences in net thrust characteristics concerning mean value and standard deviation. In this context the question arises as to which parameters mainly are responsible for that nonlinear

Table 7 Net thrust mean values and standard deviations

Inlet design	ER	μ	σ	Choking risk
Initial design:	0.4	130.41	113.81	<0.5%
$\alpha_1 = 7.5$ deg	0.6	214.63	112.66	17.3%
$\alpha_2 = 11.5$ deg	0.8	346.84	125.33	61.6%
$A_0/A_{31} = 6$	1.0	459.22	131.53	91.3%
Modified design:	0.4	155.62	114.01	<0.5%
$\alpha_1 = 6.25$ deg	0.6	247.2	115.64	31.1%
$\alpha_2 = 7.75$ deg	0.8	303.99	146.57	60.8%
$A_0/A_{31} = 5$	1.0	281.60	166.42	82.2%

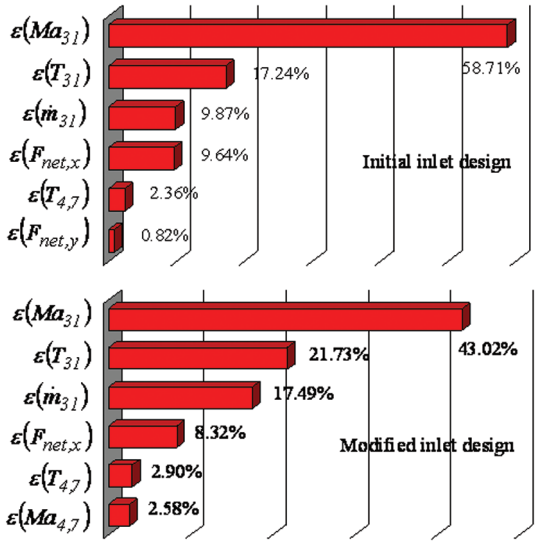

Fig. 10 Pareto plots of epistemic uncertainty.

behavior? The systems sensitivity to the specific quantified uncertainties is derived from a corresponding Pareto analysis. For the chosen configurations the overall performance is mainly influenced by the epistemic uncertainties, whereas the sum of aleatory uncertainties of flight or fuel conditions are responsible for less than 2% of the total variance in net thrust. In Fig. 10 the influences of the specific parameter variations on the net thrust in the x direction are compared for both the initial and the modified inlet design. It is concluded that the error in the mass averaged inlet outflow Mach number is responsible for 58.71% of the resulting uncertainty of the net thrust for the initial inlet design. For the modified inlet the impact of the Mach number error in the inlet outflow cross section is reduced to 43.02% but remains the most important uncertainty factor in net thrust prediction. Furthermore, the error in the inlet mass flow and mass averaged static temperature gain in importance for the modified configuration.

As mentioned previously the AoA dominates the inlet characteristics within the aleatory uncertainties. This increased sensitivity is owed to the higher length of the inlet and the associated higher variability of the shock position. The shock angles again determine the inlet outflow temperature and Mach number and via the contraction ratio the captured mass flow, too. As the weaker shock angles of the modified inlet cause lower temperature and captured mass flow, the impact of the attached model error increases. Then again the inlet outflow Mach number increases, so the impact of the error related to the inlet Mach number prediction decreases.

For both configurations the inlet is the component showing the highest sensitivity regarding both the aleatory uncertainties represented by the angle of attack and the epistemic uncertainty in mass flow, static temperature, and Mach number in the inlet outflow cross section.

VI. Conclusions

A probabilistic analysis of a scramjet propulsion system has been presented introducing a straightforward approach for uncertainty quantification. The described methodology combines the natural variance, the so-called aleatory uncertainty, and the model imperfection, the so-called epistemic uncertainty. Several inlet and combustor designs have been investigated with respect to the net thrust performance comparing deterministic and probabilistic prediction. It was found that equivalence ratios greater than 0.4 hold the risk of thermal choking. For a generic 2-D inlet with ramp angles of $\alpha_1 = 7.5$ deg and $\alpha_2 = 11.5$ deg, respectively, and a contraction ratio of 6 the probabilistic mean net thrust is higher than the deterministic value for a certain equivalence ratio, but both standard deviation and risk of thermal choking increase with greater equivalence ratios. A modified inlet design with smaller ramp angles and a lower contraction ratio is applied to reduce inlet drag and thereby increase net thrust. The *deterministic* analysis of that configuration yields a *higher* net thrust which reinforces that assumption; however, the *probabilistic* analysis yields a *lower* net thrust considering equivalence ratios greater than 0.6. In addition, the standard deviations obtained from the probabilistic analysis suggest a higher net thrust variance for the modified inlet than for the initial design. The inlet module is identified to be responsible for the bigger part of the net thrust scattering as for the inlets individual sensitivity to variations in angle of attack and the increased overall sensitivity to the inlet modules epistemic uncertainty.

This work demonstrates the benefits of probabilistic methods in hypersonic system design and is to be seen as a first step toward robust scramjet design. It clarifies the risk of sole module optimization in the presence of uncertainty. The presented first-order sensitivity studies of the occurring uncertainties impact imply further higher order interactions that will be assessed by future design of experiment studies. Furthermore multi-objective optimization techniques accounting for aleatory as well as epistemic uncertainty will be applied to maximize engine performance and simultaneously minimize net thrust variation or the risk of thermal choking.

Acknowledgments

The authors would like to thank the members and associates of the research training group Graduiertenkolleg (GRK) 1095/1 for providing their qualification data and the German Research Council (DFG) for the financial support of the project.

References

[1] Gaisbauer, U., Weigand, B., Reinartz, B., Kau, H-P., and Schröder, W., "Research Training Group GRK 1095/1: Aero-Thermodynamic Design of a Scramjet Propulsion System," International Symposium on Air Breathing Engines Paper ISABE-2007-1131, 2007.

[2] Schütte, G., and Staudacher, S., "Non-Deterministic Analysis of a Scramjet Propulsion System," CEAS-2007-366, 2007.

[3] Mantis, G. C., Mavris, D. N., "A Bayesian Approach to Non-Deterministic Hypersonic Vehicle Design," SAE Paper 2001-01-3033, 2001.

[4] Stratford, B. S., and Beavers, G. S., "The Calculation of the Compressible Turbulent Boundary Layer in an Arbitrary Pressure Gradient—A Correlation of Certain Previous Methods," N.G.T.E. Memorandum M.330-A.R.C. 21,399, British Aeronautical Research Council, London, 1961.

[5] Cebeci, T., and Bradshaw, P., *Physical and Computational Aspects of Convective Heat Transfer*, Springer–Verlag, New York, 1984.

[6] Gassner, G., Lörcher, F., and Munz, C.-D., "A Contribution of the Construction of Diffusion Fluxes for Finite Volume and Discontinuous Galerkin Schemes," *Journal of Computational Physics*, Vol. 224, No. 2, 2007, pp. 1049–1063. doi:10.1016/j.jcp.2006.11.004

[7] White, W. B., Johnson, S. M., and Dantzig, G. B., "Chemical Equilibrium in Complex Mixtures," *Journal of Chemical Physics*, Vol. 28, No. 5, 1958, pp. 751–755. doi:10.1063/1.1744264

[8] Curran, E. T., and Murthy, S. N. B., *Scramjet Propulsion*, Progress in Astronautics and Aeronautics, Vol. 189, AIAA, Reston, VA, 2000, Chap. 10.

[9] Chun, J., Scheuermann, T., von Wolfersdorf, J., and Weigand, B., "Experimental Study on Combustion Mode Transition in a Scramjet with Parallel Injection," AIAA Paper 2006-8063, 2006.

[10] Ferson, S., and Ginzburg, L. R., *Different Methods are Needed to Propagate Ignorance and Variability*, Reliability Engineering and System Safety, Vol. 54, Elsevier, in association with the European Safety and Reliability Association, and the Safety Engineering and Risk Analysis Division, Amsterdam, The Netherlands, 1996, pp. 133–144.

[11] Mantis, G. C., "Quantification and Propagation of Disciplinary Uncertainty via Bayesian Statistics," Ph.D. Dissertation, Georgia Institute of Technology, Atlanta, GA, 2002.

[12] Jaynes, E. T., "Information Theory and Statistical Mechanics," *Physical Review*, Vol. 106, No. 4, 1957, pp. 620–630. doi:10.1103/PhysRev.106.620

[13] Qiying, W., Bing-Yi, J., and Lincheng, Z., "The Berry Esséen Bound for Studentized Statistics," *The Annals of Probability*, Vol. 28, No. 1, 2000, pp. 511–535. doi:10.1214/aop/1019160129

[14] Bae, H.-R., Grandhi, R. V., and Canfield, R. A., "Uncertainty Quantification of Structural Response Using Evidence Theory," *AIAA Journal*, Vol. 41, No. 10, Oct. 2003, pp. 2062–2068. doi:10.2514/2.1898

[15] Loeven, G. J. A., Witteveen, J. A. S., and Bijl, H., "Probabilistic Collocation: An Efficient Non-Intrusive Approach for Arbitrarily Distributed Parametric Uncertainties," *45th AIAA Aerospace Sciences Meeting and Exhibit*, AIAA, Reston, VA, 8–11 Jan. 2007.

[16] Fahrmeir, L., Künstler, R., Pigeot, I., and Tutz, G., *Statistik. Der Weg zur Datenanalyse*, Springer Educational Series, Springer, New York, 2003.

[17] Lorenz, E. N., "Deterministic Non-Periodic Flow," *Journal of the Atmospheric Sciences*, Vol. 20, No. 2, 1963, pp. 130–141. doi:10.1175/1520-0469(1963)020<0130:DNF>2.0.CO;2

[18] Kullback, S., and Leibler, R. A., "On Information and Sufficiency," *Annals of Mathematical Statistics*, Vol. 22, No. 1, 1951, pp. 79–86. doi:10.1214/aoms/1177729694

[19] Kreutz, M., "Modellierung Unvollständig Beschriebener Systeme," Ph.D. Dissertation, Insitute of Neuroinformatics at the Ruhr Univerität Bochum, Bochum, Germany, 1999.

[20] Häberle, J., and Gülhan, A., "Investigation of the Performance of a Scramjet Inlet at Mach 6 with Boundary Layer Bleed," AIAA Paper 2006-8139, 2006.

[21] Häberle, J., "Investigation of the Flow Field of a 2D Scramjet Inlet at Mach 7 with Optional Boundary Layer Bleed," AIAA Paper 2007-5068, 2007.

[22] Krause, M., and Ballmann, J., "Numerical Solutions and Design of a Scramjet Intake Using Two Different RANS Solvers," AIAA Paper 2007-5423, 2007.

[23] Chun, J., Scheuermann, T., von Wolfersdorf, J., and Weigand, B., "Experimental Study on Combustion Mode Transition in a Scramjet with Parallel Injection," AIAA Paper 2006-8063, 2006.

[24] Gerlinger, P., Kasal, P., Schneider, F., von Wolfersdorf, J., Weigand, B., and Aigner, M., "Experimental and Numerical Investigation of Lobed Strut Injectors for Supersonic Combustion," *Basic Research and Technologies for Two-Stage-to-Orbit Vehicles*, Colloborative Research Centers, Wiley, New York, 2005.

[25] Kindler, M., Gerlinger, P., and Aigner, M., "Numerical Investigations of Mixing Enhancement by Lobed Strut Injectors in Turbulent Reactive Supersonic Flows," ISABE Paper ISABE-2007-1314, 2007.

[26] Hirschen, C., and Gülhan, A., "Experimental Study of a Scramjet Nozzle Flow Using the Pressure Sensitive Paint Method," *Journal of Propulsion and Power* (to be published).

[27] Space Age Control, Inc., Heated, High Speed Air Data Boom, Product No. 100700, 2002.

[28] International Electrotechnical Commission (IEC), Pt100 Thermocouple, Class B, IEC 751, 2000.

[29] Kulite, Inc., Miniature Pressure Transducer, Product No. XCQ-080.

[30] Göing, M., "Nozzle Design Optimization by Method-of-Characteristics," AIAA Paper 90-2024, 1990.

[31] Smart, M. K., "Optimization of Two-Dimensional Scramjet Inlets," *Journal of Aircraft*, Vol. 36, No. 2, March–April 1999, pp. 430–433. doi:10.2514/2.2448

[32] Saliby, E., "Descriptive Sampling: An Improvement Over Latin Hypercube Sampling," *Proceedings of the 29th Conference on Winter Simulation*, 1997, pp. 230–233.

R. Bowersox
Associate Editor